

Three-dimensional imaging of colloidal glasses under steady shear

R. Besseling¹, Eric R. Weeks², A. B. Schofield¹, W. C. K. Poon¹

¹ Scottish Universities Physics Alliance (SUPA) and School of Physics,

The University of Edinburgh, Kings Buildings, Mayfield Road, Edinburgh EH9 3JZ, United Kingdom.

² Physics Department, Emory University, Atlanta, Georgia 30322, USA.

(May 25, 2019)

Using fast confocal microscopy we image the three-dimensional dynamics of particles in a colloidal glass under continuous, steady shear. The quiescent glass, with particles permanently caged by neighbors, shear-melts into an ergodic state in which successive plastic cage rearrangements lead to nearly isotropic diffusion at long times. For small shear rate $\dot{\gamma}$ the inverse structural relaxation time $\tau_\alpha^{-1}(\dot{\gamma})$ and diffusivity increase linearly with $\dot{\gamma}$ ('ideal' shear thinning), but for larger $\dot{\gamma}$ they increase only *sub-linearly*, as predicted theoretically and seen in simulations of model glasses. Microscopically, the plastic rearrangements are heterogeneous for $t \lesssim \tau_\alpha$ and appear cooperative in nature.

Glassy materials are ubiquitous in nature and in industry, ranging from molecular and metallic glasses [1,2] to soft glasses like colloidal suspensions, emulsions and foams [3,4]. Of special importance, both practically and fundamentally, is their deformation and flow (or rheology). While their microstructure is disordered and liquid-like, mechanically they are solids, with finite shear moduli and yield stresses. Post yield, their flow is highly non-Newtonian even at the smallest shear rates, $\dot{\gamma}$, showing intriguing effects like stress overshoots and shear banding [2–4]. Various theories [4–6] have addressed these effects but direct experimental checks of the *microscopic* processes these theories propose are scarce. Experiments on soft glasses are beginning to address this issue, but have been restricted to coarse grained information, two dimensional (2D) or interrupted flows or ordering phenomena [7–10]. Simulations have thus been the main tool to date for validating theoretical proposals concerning microscopic behavior in glassy flow [11,12].

Deformation at constant $\dot{\gamma}$ ('steady shear'), which is predicted to induce a non-equilibrium ergodic state [13], is the best studied type of non-linear glassy rheology [4,5]. Starting from a model for shear-induced microscopic relaxation, Mode Coupling Theory (MCT) can make detailed predictions concerning steady-shear glassy rheology, including a limiting yield stress at $\dot{\gamma} \rightarrow 0$ [14]. In addition, simulations show that the microscopic relaxations under these conditions are spatially heterogeneous [6,12]. In this Letter we report a three-dimensional (3D) imaging study of a colloidal glass under steady shear. Our detailed single-particle real-time data broadly confirm theory and simulation, and provide an experimental foundation for relating microscopic behavior to various aspects of bulk rheology.

Our system consists of sterically-stabilized polymethylmethacrylate (PMMA) particles (radius $a = 850\text{nm}$, determined by light scattering, polydispersity $\lesssim 10\%$ [15]) fluorescently labelled with nitrobenzoxadiazole and sus-

pended in a mixture of cycloheptyl bromide and decalin (viscosity $2.6\text{ mPa}\cdot\text{s}$) for simultaneous density and refractive index matching. In this medium particles acquire a small charge [16] which is largely screened by adding 4 mM tetrabutylammonium chloride, leading to nearly hard-sphere (HS) behavior, with a glass transition (determined from mean-squared displacements, see below) occurring at volume fraction $\phi_g \simeq 0.58$ [17]; we work at $\phi \simeq 0.61$ (determined by imaging) [18]. The dimensionless shear rate, or Peclet number, is $\text{Pe} = 4a^2\dot{\gamma}/D_0$, with D_0 the bare diffusion coefficient. Our experiments cover $0.01 < \text{Pe} < 0.1$. Note that in terms of the Brownian time $\tau_B = a^2/6D_0$ ($= 1.24\text{ s}$ in our system), $\text{Pe} = 24\dot{\gamma}\tau_B$.

We employ a linear parallel plate shear-cell with a plate separation $\sim 400\text{ }\mu\text{m}$, parallel to $\pm 1\%$ over a $\sim 100\text{ mm}^2$ drop confined between the plates by surface tension. x , y and z denote the velocity, vorticity (or neutral) and gradient directions respectively. The top plate is driven at $0.1 - 10\mu\text{m/s}$ by a mechanical actuator with magnetic encoder, and steady shear is applied for a finite, but long, time. The maximum total accumulated shear is limited by cell design to $\Delta\gamma \lesssim 1000\%$. Boundary slip, which occurred when using bare glass slides, was prevented by coating the slides with particles (1–3 disordered monolayers) [19]. A solvent bath minimized evaporation.

A $30\text{ }\mu\text{m} \times 30\text{ }\mu\text{m} \times 15\text{ }\mu\text{m}$ volume in the drop (containing $N \sim 3000$ particles) was imaged from below as a stack of 75 slices using a fast confocal microscope (VTEye, Visitech International). The scanning of each 3D stack took $\sim 2\text{ s}$. In each stack, particles were located with resolution $\delta x, \delta y \sim 40\text{ nm}$ and $\delta z \sim 100\text{ nm}$ [20]. Particle tracking from frame to frame was achieved by first subtracting from the raw coordinates a time (t) dependent x -displacement profile, measured via stack-wise correlation analysis of raw images, and adding this back after particle tracking. The resulting x -displacements over a given time interval dt , $\{\Delta x_i(z_i, dt)\}$ ($i = 1$ to N), always have an average linear dependence on z . From

this we checked that the sample in our imaged volume was indeed subjected to uniform shear, and measured the actual shear rate $\dot{\gamma}$, which may be different from the nominal applied shear rate due to shear banding. These effects will be reported elsewhere; here we focus on steady states observed in a region from $15 - 30 \mu\text{m}$ above the cover slide with a linear velocity profile. We also checked, via bond-order analysis [21], that shear-induced crystallization [22] was absent for our range of $\dot{\gamma}$.

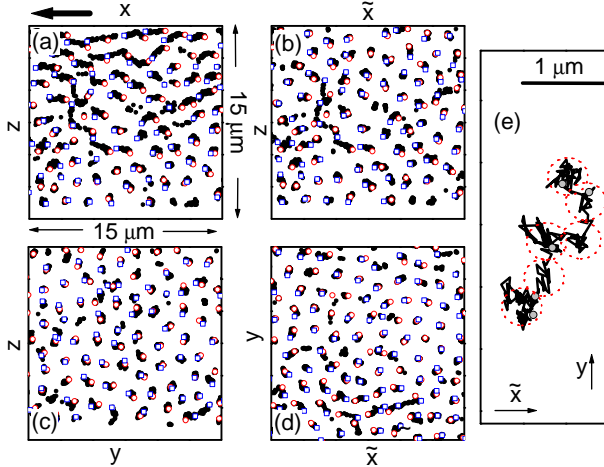


FIG. 1. Particle trajectories for $\dot{\gamma} = 0.93 \times 10^{-3} \text{ s}^{-1}$. (a) $1.5 \mu\text{m}$ thick slice in the x,z plane over 160 s; the start of the trajectories is shown by red circles; the end by blue squares. The big arrow marks the shear direction. (b) As in (a) but in the desheared, \tilde{x},z , reference frame, with $\tilde{x}_i = x_i - \dot{\gamma} \int_0^t z_i(t') dt'$. (c) y,z plane over 160 s. (d) \tilde{x},y plane over 160 s. (e) Single trajectory in the \tilde{x},y plane over 800 s. Dotted circles indicate rattling in several cages (not the particle size), grey dots mark the locations at $t = 0, 200, 400, 600, 800$ s.

Figure 1(a) shows the trajectories in an x,z slice at $\dot{\gamma} = 0.93 \times 10^{-3} \text{ s}^{-1}$. The displacement gradient due to shear is evident. To highlight the shear-induced dynamics, we show in Fig. 1(b) the *non-affine* component of the motion obtained by subtracting the uniform shear via $\tilde{x}_i = x_i - \dot{\gamma} \int_0^t z_i(t') dt'$. Considerable shear-induced non-affine displacements are seen in this plane as well as in the other planes, Figs. 1(c,d). On the time scale considered here, these rearrangements are heterogeneous; similar heterogeneities are seen in *quiescent* systems below the glass transition [23]. Zooming in on a single particle, Fig. 1(e), we observe that its dynamics under shear consists of intervals of cage ‘rattling’, interrupted by shear-induced plastic cage-breaking events.

We next explore the structural relaxation by calculating the self-intermediate scattering function, $F_s(Q, t) = \langle \cos(Q[y_i(t_0+t) - y_i(t_0)]) \rangle_{i,t_0}$, for $Q = Q_m \simeq 3.8a^{-1}$ (the peak in the structure factor obtained from the data). In Fig. 2 we show results for the scattering vector $\vec{Q} \parallel y$, i.e. in the neutral direction [11,12], but the results (not

shown) for $\vec{Q} \parallel z$ and x (using the non-affine displacements \tilde{x}_i for the latter) are similar. F_s for the quiescent glass ($\dot{\gamma} = 0$) decays very little over our observation window, reflecting caging of particles by their neighbors; at longer times aging was observed [10,24]. The short time decay due to initial cage exploration ($t \lesssim \tau_B$ [25]) is inaccessible in our experiments. At small $\dot{\gamma}$, F_s at short times still exhibits a plateau, in agreement with the caging observed in Fig. 1(e). This plateau shrinks with increasing $\dot{\gamma}$. At longer times, F_s decays strongly for all $\dot{\gamma} \neq 0$, signaling shear-induced structural relaxation due to cage rearrangements. The structural, or α , relaxation time τ_α , defined by $F_s(Q_m, t = \tau_\alpha) = e^{-1}$, decreases on increasing $\dot{\gamma}$. Importantly, F_s is independent of the starting time t_0 (see data for $\dot{\gamma} = 0.93 \times 10^{-3} \text{ s}^{-1}$), i.e., a stationary non-equilibrium state is achieved. The complete decay of F_s in the y , Fig. 2, and in the x,z directions (not shown) evidences the full fluidization of the sheared glass.

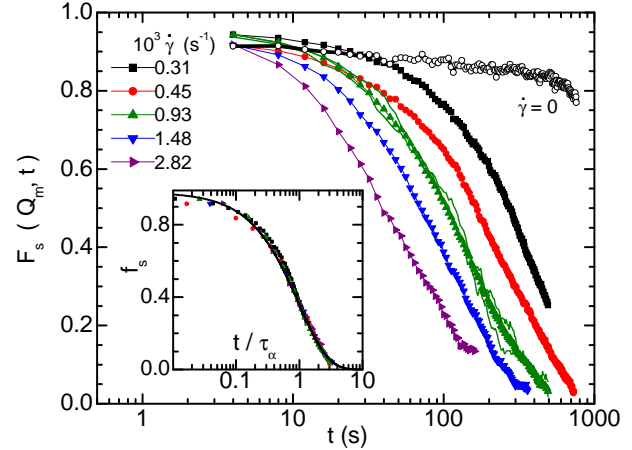


FIG. 2. Self intermediate scattering function, $F_s(Q_m, t)$, with $\dot{\gamma}$ increasing from top to bottom. Thin lines for the data at $\dot{\gamma} = 0.93 \times 10^{-3} \text{ s}^{-1}$ represent two of the curves used in the average, with time origins t_0 separated by 180 s ($\sim 1.2\tau_\alpha$). Inset: master curve $f_s(Q_m, t/\tau_\alpha)$, showing collapse of F_s when time is scaled by the structural relaxation time $\tau_\alpha(\dot{\gamma})$. Drawn line: Kolrausch form $f_s \propto \exp[-(t/\tau_\alpha)^\beta]$ with $\beta = 0.95$.

The time-shear superposition principle [5,14] predicts that when time is scaled by τ_α , the long time structural decay should follow a master curve $f_s(Q, t/\tau_\alpha)$. This is indeed observed (Fig. 2 inset). Moreover, f_s exhibits nearly exponential decay (see figure caption), in agreement with simulations of Lennard-Jones (LJ) glasses [11].

We now consider the dependence of τ_α on the shear rate. At low $\dot{\gamma}$, $\tau_\alpha \sim \dot{\gamma}^{-1}$, Fig. 3(a). In this regime, the accumulated strain at τ_α , $\delta\gamma_\alpha = \tau_\alpha \dot{\gamma} \simeq 11\%$, matching the yield strain and ‘maximum recovered strain’ obtained from bulk rheology [26]. Similar $\delta\gamma_\alpha$ values are also found in simulated LJ glasses at low $\dot{\gamma}$ [11]. Deviations from $\tau_\alpha \sim \dot{\gamma}^{-1}$ scaling are observed at higher $\dot{\gamma}$, Fig. 3(a), as the increasingly rapid α relaxation process encroaches on β relaxation processes in the 1 to 10 s time window (cf.

Fig. 2). Equivalently, deviations should set in when $\dot{\gamma}^{-1}$ becomes comparable to the strain relaxation time, τ_γ , measured in step stress experiments in [26]; at $\phi = 0.62$, $\tau_\gamma \sim 10^3 \tau_B$ [26], giving $\tau_\gamma \lesssim 10^3$ s in our system. We indeed see deviations for $\dot{\gamma} \gtrsim 10^{-3}$ s $^{-1}$, Fig. 3(a).

Identifying τ_α as a measure for the viscosity [14], we then obtain a dimensionless measure for the stress $\bar{\sigma} = \dot{\gamma} \tau_\alpha(\dot{\gamma})$ [27]. The inferred 'flow curve', $\bar{\sigma}(\dot{\gamma})$, has a plateau at low $\dot{\gamma}$ and turns up at larger $\dot{\gamma}$, Fig. 3(b), crossing over at $\text{Pe} \simeq 0.02$. Such features are indeed observed in experimental flow curves of colloidal glasses [26,28], MCT calculations [14] and simulated LJ glasses [11,27], suggesting they may be universal for glassy rheology [29].

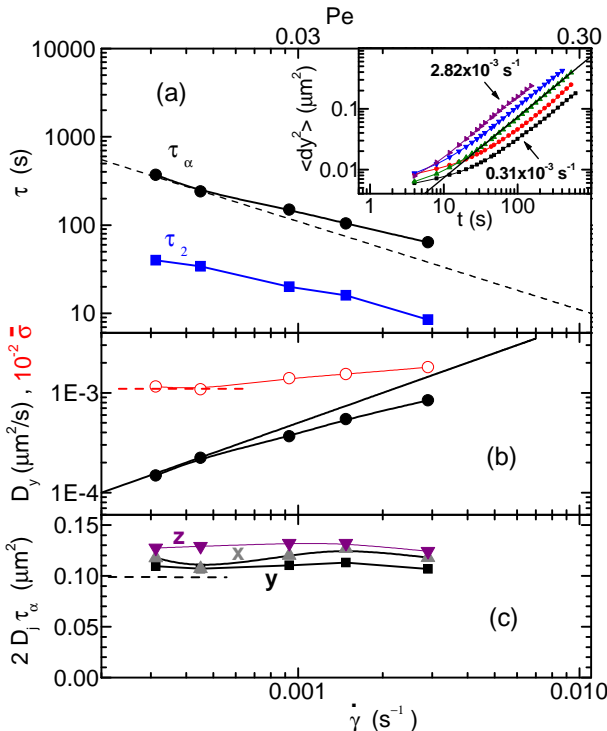


FIG. 3. (a) Structural relaxation time (●) and the characteristic time τ_2 for the crossover from caged to diffusive behavior (squares) vs. $\dot{\gamma}$; dashed line gives $\tau_\alpha = 0.11/\dot{\gamma}$. Inset: mean square displacement in the vorticity direction for shear rates as in Fig. 2. Line: $\langle dy^2(t) \rangle = 2D_y t$ for $\dot{\gamma} = 0.93 \times 10^{-3}$ s $^{-1}$. (b) (●) Diffusion constant D_y vs. $\dot{\gamma}$. Line: $D_y/a^2 = 0.69\dot{\gamma}$. (○) Dimensionless stress $\bar{\sigma} = \dot{\gamma}\tau_\alpha$ (see text). (c) The scaled diffusion constant $2D_j\tau_\alpha \simeq \langle dr_j^2(\tau_\alpha) \rangle$ vs. $\dot{\gamma}$ for $j = x, y, z$. The dashed line indicates the value expected for gaussian displacements $\langle dy^2(\tau_\alpha) \rangle = 2/Q_m^2$.

As a second 'ensemble' characterization we study the mean squared displacement (MSD) and examine the anisotropy of the non-affine component of the plastic motion. In the inset to Fig. 3(a) we first show $\langle dy^2(t) \rangle$ for the various shear rates. It exhibits a crossover from caged to diffusive motion for $\sqrt{\langle dy^2 \rangle}/a \simeq 0.15$ ($\langle dy^2 \rangle \simeq 0.016$ μm 2), in reasonable agreement with the 'Lindemann parameter' measuring the amount of cage rattling at the

quiescent glass transition [17]. The long time diffusion constant D_y , Fig. 3(b), essentially follows the relaxation rate τ_α^{-1} , and not the shear rate $\dot{\gamma}$. To show this more clearly and to address the issue of anisotropy, we plot in Fig. 3(c) the product $2D_j\tau_\alpha$ for the three directions ($j = x, y, z$) along with the value $\langle dy^2(\tau_\alpha) \rangle = 2/Q_m^2$ expected from a gaussian approximation $F_s(Q_m, t) \simeq e^{-Q_m^2 \langle dy^2(t) \rangle / 2}$ [25]. The value for $2D_y\tau_\alpha$ agrees well with $2Q_m^{-2}$ and this gaussian long time behavior also occurs in the other directions [30]. More importantly, the diffusion constants exhibit only a mild anisotropy: while D_z is larger than $D_{x,y}$, the difference is at most $\sim 20\%$. Similar or even smaller anisotropy has been observed in various simulations of sheared, glassy systems [12,31]. Moreover, isotropic shear-induced diffusion is also observed in *dilute* suspensions [32]. In contrast, sheared *non-Brownian* suspensions ($\text{Pe} \rightarrow \infty$) exhibit a pronounced anisotropy ($D_x/D_{y,z} \sim 8$) [33], with a value for D_x very close to our small $\dot{\gamma}$ limiting behavior $D/(a^2\dot{\gamma}) \simeq 0.7$.

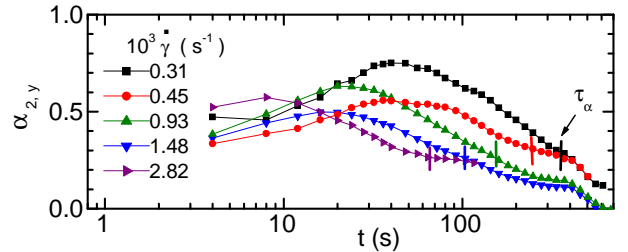


FIG. 4. Nongaussian parameter α_2 of the time-dependent probability distribution of displacements $P(dy(t))$ for the various shear rates. Markers indicate the α -relaxation time.

The dynamics can be further characterized via the non-gaussian parameter $\alpha_{2,j} = \langle dr_j^4(t) \rangle / 3 \langle dr_j(t)^2 \rangle^2 - 1$ for the probability distribution of the displacements $P(dr_j(t))$ [23]. For a gaussian distribution, $\alpha_2 = 0$; larger values of α_2 indicate broad tails in $P(dr_j(t))$, reflecting cage rearranging motions such as in Fig. 1(e). In Fig. 4 we show $\alpha_{2,y}(t)$ for the various shear rates. It exhibits a peak at a time τ_2 [34] corresponding to the crossover from caged to diffusive behavior in the MSD (inset, Fig. 3(a)), and vanishes for longer times, consistent with the near exponential form of f_s , Fig. 2 inset. A non-zero α_2 is associated with cooperativity, in our case, in the motions leading to cage rearrangement. Such cooperativity is consistent with the heterogeneities observed in the trajectories in Fig. 1 (b)-(d) for $t < \tau_\alpha$. In fact, a preliminary analysis (not shown) of subsets of particles with large non-affine displacements $|dr(\tau_2)|$ also clearly revealed clustering. Such clusters may be related to the 'Shear Transformation Zones' proposed to account for plastic flow in other amorphous solids like metallic glasses [6].

The crossover time τ_2 decreases systematically with $\dot{\gamma}$ (Fig. 3(a)), albeit with a slightly different $\dot{\gamma}$ -dependence than that of τ_α . The associated accumulated strain $\dot{\gamma}\tau_2$

increases from $\sim 1.3\%$ to $\sim 2.5\%$. This is comparable to the strain amplitudes at which nonlinearity sets in in measurements of the storage modulus of HS glasses [7]. Interestingly, these strains are somewhat less than the maximum elastic strain $\gamma_{\text{el}}^{\text{max}}$ in our system estimated from the average surface-to-surface spacing of particles [7]: $\gamma_{\text{el}}^{\text{max}} = 1 - (\phi/\phi_{\text{rcp}})^{1/3} = 3.6\%$ (with $\phi_{\text{rcp}} \simeq 0.68$ our random close packing fraction measured via imaging).

By way of a summary, we seek to connect all the strands for one specific shear rate, $\dot{\gamma} = 0.93 \times 10^{-3} \text{s}^{-1}$. At this $\dot{\gamma}$, $\tau_\alpha \simeq 150 \text{ s}$, Figs. 2 and 3(a). The trajectory in Fig. 1(e) covers 800 s and involves ≈ 6 cage rearrangements, giving an average cage rearrangement time $\lesssim 150 \text{ s} \approx \tau_\alpha$. The strain accumulated at this time is $\sim 14\%$, similar to the yield strain seen in rheology. At this $\dot{\gamma}$, deviations from the low- $\dot{\gamma}$ behavior of $\tau_\alpha \propto \dot{\gamma}^{-1}$ begin to set in, Fig. 3(a), associated with straining the sample at a rate faster than the inverse intrinsic strain relaxation time τ_γ^{-1} . The maximum non-gaussian behavior occurs for $t = \tau_2 \simeq 20 \text{ s} \ll \tau_\alpha$, Fig. 4, when the MSD enters the long-time diffusive regime, Fig. 3(a) inset.

In conclusion, we observe that a slowly sheared colloidal glass fluidizes via plastic cage rearrangements. The associated *non-affine* motion is nearly isotropic and causes structural relaxation and diffusion at a rate τ_α^{-1} which initially increases linearly with $\dot{\gamma}$, but grows only sub-linearly for larger $\dot{\gamma}$. Moreover, for $t < \tau_\alpha$ the plastic rearrangements are heterogeneous and occur cooperatively. Noteworthy, many of the features we observe in a colloidal *hard-sphere* glass agree with simulations of *Lennard-Jones* glasses. Our measurements provide a microscopic picture of various macroscopic rheological phenomena and open the way for further testing various theories to describe nonlinear glassy rheology.

We thank J. Bergenholz, M. E. Cates, M. Fuchs, P. Pusey and G. Petekidis for helpful discussions. UK and US work was funded by EPSRC GR/S10377/01 and NSF Grant No. DMR-0239109 respectively.

D. Derks *et al.*, J. Phys. Cond. Mat. **16**, 3917 (2004); I. Cohen *et al.*, Phys. Rev. Lett. **93**, 046001 (2004).

[10] D. Bonn *et al.*, Phys. Rev. Lett. **89**, 015701 (2002).

[11] L. Berthier and J.L. Barrat, Phys. Rev. Lett. **89**, 095702 (2002); J. Chem. Phys. **116**, 6228 (2002).

[12] R. Yamamoto and A. Onuki, Phys. Rev. E **58**, 3515 (1998); Phys. Rev. Lett. **81**, 4915 (1998).

[13] L.F. Cugliandolo *et al.*, Phys. Rev. E **55**, 3898 (1997). J.L. Barrat and L. Berthier, Phys. Rev. E **63**, 012503 (2000).

[14] M. Fuchs and M.E. Cates, Phys. Rev. Lett. **89**, 248304 (2002); Far. Disc. **123**, 267 (2003). See also K. Miyazaki and D.R. Reichman, Phys. Rev. E **66**, 050501(R) (2002).

[15] This was deduced from the very slow crystallization of the quiescent samples for $\phi \gtrsim 50\%$.

[16] A. Yethiraj and A. van Blaaderen, Nature **421** 513 (2003).

[17] The long-time rms-displacement at ϕ_g is $\sqrt{\langle dy^2 \rangle}/a \simeq 0.13$; the HS value is $\simeq 0.18$ [25].

[18] ϕ for different experimental runs varied by $\pm 1\%$, causing fluctuations in the various calculated quantities without affecting the trends discussed.

[19] The coating also suppresses wall induced ordering as may occur in glassy suspensions near untreated surfaces.

[20] J.C. Crocker and D.G. Grier, J. Col. Int. Sc. **179**, 298 (1996). At our frame rate, shear-induced distortions in the x, z plane are unimportant for $\dot{\gamma} \lesssim 0.05 \text{ s}^{-1}$.

[21] P.R. ten Wolde *et al.*, J. Chem. Phys **104**, 9932 (1996); The average number of crystalline bonds per particle was $\langle N_x \rangle \sim 2.5$ and constant in time, with small clusters of crystalline particles (with $N_x \geq 8$) fluctuating spatially and temporally without signs of growth.

[22] B.J. Ackerson and P.N. Pusey, Phys. Rev. Lett. **61**, 1033 (1988); M.D. Haw *et al.*, Phys. Rev. E **57**, 6859 (1998). We observed (partial) crystallization for faster ($\dot{\gamma} \gtrsim 0.1 \text{ s}^{-1}$) steady shear or sawtooth oscillatory shear with a strain amplitude $\sim 100\%$.

[23] E.R. Weeks *et al.*, Science **287**, 627 (2000); W.K. Kegel and A. van Blaaderen, Science **287**, 290 (2000).

[24] R.E. Courtland and E.R. Weeks, J. Phys. Cond. Mat. **15** S359 (2003).

[25] W. van Megen *et al.*, Phys. Rev. E **58**, 6073 (1998).

[26] G. Petekidis *et al.*, J. Phys. Cond. Mat. **16**, 3955 (2004).

[27] F. Varnik and O. Henrich, cond-mat/0511714. Here the relation $\bar{\sigma} = \dot{\gamma}\tau_\alpha \propto \sigma$ was justified via direct simulation.

[28] M. Fuchs and M. Ballauff, J. Chem. Phys. **122**, 094707 (2005).

[29] Generally, we expect $\dot{\gamma}$ at the crossover (or, alternatively, τ_γ) to depend on the microscopic dynamics and the 'distance' to the quiescent glass transition, see [26,27] and O. Henrich *et al.*, J. Phys. Cond. Mat. **17**, s3625 (2005).

[30] Taking $\tau_{\alpha,j}$ evaluated from $F_s(Q_m \parallel j, t = \tau_{\alpha,j}) = 1/e$, yields $D_j \tau_{\alpha,j} \simeq 0.11$ independent of j .

[31] D.L. Malandro and D.J. Lacks, Phys. Rev. Lett. **81**, 5576 (1998); K. Miyazaki *et al.*, Phys. Rev. E **70**, 011501 (2004).

[32] X. Qiu *et al.*, Phys. Rev. Lett. **61**, 2554 (1988).

[33] V. Breedveld *et al.*, J. Chem. Phys. **116**, 10529 (2002).

[34] The peak height of α_2 shows some scatter, which may be due to the slight variations in volume fraction [18].